Gas Sorption Properties of a New Three-Dimensional In-ABDC MOF With a Diamond Net

In-Hwan Choi[1], Suk Bin Yoon[1], So-Young Jang[1], Seong Huh[1]*, Sung-Jin Kim[2] and Youngmee Kim[2]*

[1] Department of Chemistry and Protein Research Center for Bio-Industry, Hankuk University of Foreign Studies, Yongin, South Korea, [2] Department of Chemistry and Nano Science and Institute of Nano-Bio Technology, Ewha Womans Univeristy, Seoul, South Korea

The pseudotetrahedral node, $[In(O_2CR)_4]^-$, often found in In^{III}-based metal-organic frameworks (MOFs) without a cluster-based secondary building unit (SBU) is a negatively charged center due to charge mismatch between an 8-coordinate In^{III} ion and four anionic carboxylate bridging ligands. Thus, In-MOFs with this pseudotetrahedral node tend to bear a counter-cation near each In^{III} center in the frameworks. Generally, dialkylammonium-based cations such as $Me_2NH_2^+$ and $Et_2NH_2^+$ directly derived from N,N-dimethylformamide (DMF) or N,N-diethylformamide (DEF) solvents during MOF formation reactions play a significant role to form a stable framework through charge matching. If these cations thermally derived from DMF or DEF were not suitable for crystal growth of In-MOFs, it becomes very challenging to obtain high quality single crystals for X-ray structure determination of the frameworks. In this context, high quality crystals of In-ABDC MOF were not easily prepared from a ditopic azobenzene-4,4'-dicarboxylic acid (H_2ABDC) through a thermal reaction in DMF or DEF. We successfully overcome this problem by employing a room-temperature ionic liquid, 1-ethyl-3-methylimidazolium tetrafluoroborate ([EMIM][BF_4]), and the resulting three-dimensional (3D) In-ABDC MOF, $[EMIM][In(ABDC)_2]\cdot DEF\cdot H_2O$ (**I**), was structurally characterized by X-ray diffraction. The 3D framework indicates a 4-connected uninodal net with Schläfli symbol of 6^6 (**dia**). The gas sorption properties of solvent-free **I** were also investigated in detail.

Keywords: metal-organic framework, indium, azobenzene-4,4'-dicarboxylic acid, carbon dioxide sorption, hydrogen sorption

INTRODUCTION

One of the most valuable features of porous metal-organic frameworks (MOFs) may lie in the formation of robust crystalline organic/inorganic hybrid materials with various functionalities (Farha and Hupp, 2010; Furukawa et al., 2013; Nguyen et al., 2013; Foo et al., 2014; Kim and Huh, 2016; Qin et al., 2017; Diercks et al., 2018). Almost all metallic elements can be utilized for the preparation of MOFs with a range of bridging ligands. The properties of a certain MOF can be come from either metallic center or functional bridging ligands (Chui et al., 1999; Kim et al., 2013; Karagiaridi et al., 2014; Beyzavi et al., 2015; Choi et al., 2016; Kim and Huh, 2016; Zhu et al., 2017). Most porous MOFs contain cluster-based secondary building units (SBUs), and these SBUs play a pivotal role in constructing large three-dimensional (3D) frameworks as

witnessed in the case of MOF-5 and MOF-177 (Li et al., 1999; Chae et al., 2004). Contrarily, metal ions such as In^{III} ion ($r = 0.80$ Å) with a large ionic radius can lead to stable mononuclear 8-coordinate center with four carboxylate-based bridging ligands to form topologically interesting multidimensional network structures. A congener of In^{III} ion with a small ionic radius such as Al^{III} ion ($r = 0.54$ Å) usually tends to form a 6-coordinate center. In In-MOFs, the anionic pseudotetrahedral node, $[In(O_2CR)_4]^-$, can be effectively formed with dicarboxylate bridging ligands in the absence of other auxiliary bridging linkers for the formation of 3D frameworks. Additionally, there should be a counter-cation near each $[In(O_2CR)_4]^-$ node because of charge matching. There are many examples of 3D In-MOFs solely derived from ditopic, tritopic, tetratopic, and pentatopic carboxylate-based bridging ligands (Sun et al., 2002; Lin et al., 2007, 2012; Huh et al., 2009; Gu et al., 2012; Yu et al., 2012; Zheng et al., 2013; Cho et al., 2014; Huang et al., 2014; Johnson et al., 2014; Wang et al., 2014; Grigoropoulos et al., 2016; Li et al., 2016; Aguirre-Díaz et al., 2017; Zhao et al., 2017; Yang et al., 2019). The most common counter-cations are either $Me_2NH_2^+$ or $Et_2NH_2^+$ which can be *in-situ* generated from the solvents: *N,N*-dimethylformamide (DMF) or *N,N*-diethylformamide (DEF). A range of ammonium-based cations can also be added into the reaction mixture to facilitate the formation of anionic In-MOFs (Chen et al., 2009; Lin et al., 2012; Huang et al., 2014; Mihaly et al., 2016; Zhao et al., 2018). In these cases, the counter-cations found in MOFs are the added ammonium-based cations.

Although the Lewis acidic open metal sites are often observed in MOFs (Chui et al., 1999), the unique and controllable functionalities of MOFs are mainly stemmed from the bridging ligands bearing diverse organic functional groups such as -NH₂, -NR₂, NR₃ of 1,4-diazabicyclo[2.2.2]octane (DABCO), imidazolyl moiety, ureido moiety, -NH-CO-, -OH, -SH, and -SO₃H (Gu et al., 2010, 2011; Zheng et al., 2011; Fracaroli et al., 2014; Phang et al., 2014, 2015; McDonald et al., 2015; Flaig et al., 2017; Baek et al., 2018; Hakimifar and Morsali, 2019; Li et al., 2019). Therefore, functional MOFs can act as either Lewis basic materials or Lewis acidic materials depending on the tethered functional groups. Especially, MOFs with well-defined Lewis basic sites can be employed in a range of advanced applications including selective heterogeneous catalysis, CO_2 capture/separation, and CO_2 conversion into cyclic organic carbonates (Beyzavi et al., 2015; He et al., 2016; Maina et al., 2017; Huh, 2019). In this context, many different types of bridging ligands containing Lewis basic moieties have been being developed and investigated. We also reported several functional MOFs with Lewis basic sites for heterogeneous catalysis for organic transformations and selective adsorption of CO_2 over other competing gases (Gu et al., 2010, 2011; Kim et al., 2013, 2017, 2018). We envision that new functional MOFs with Lewis basic functionalities are very useful materials for various applications.

There are several MOF systems containing a ditopic azobenzene-4,4'-dicarboxylate ($ABDC^{2-}$) bridging ligand in which the azo group (-N=N-) can potentially act as Lewis basic sites (Nguyen et al., 2011; Zhuang et al., 2011; Lyndon et al., 2013; Gong et al., 2015; Liu et al., 2016; Zhao et al., 2016; Yuan

et al., 2017; Xu et al., 2018; Yang et al., 2018). We expected that the assembly between In^{III} ions with $ABDC^{2-}$ bridging ligands could lead to a new In-MOF with openly accessible azo-group-based Lewis basic sites from the bridged $ABDC^{2-}$ ligands. In this study, we successfully prepared a 3D In-ABDC MOF formulated as $[EMIM][In(ABDC)_2] \cdot DEF \cdot H_2O$ (**I**) by employing a room-temperature ionic liquid, 1-ethyl-3-methylimidazolium tetrafluoroborate ($[EMIM][BF_4]$), as an auxiliary counter-cation source. The permanent porosity of solvent-free **I** was evaluated by a standard volumetric N_2 adsorption/desorption analysis at 77 K. Both CO_2 and H_2 sorption abilities of **I** were also measured at suitable temperatures.

EXPERIMENTAL SECTION

Materials

$InCl_3$ (Sigma-Aldrich), azobenzene-4,4'-dicarboxylic acid (Chemsoon), 1-ethyl-3-methylimidazolium tetrafluoroborate (TCI), tetraethylammonium bromide (Sigma-Aldrich), and *N,N*-diethylformamide (TCI) were used as received. Other reagent grade solvents were used without further purification.

Instrumentation

Thermogravimetric analysis was carried out on a TGA Q5000 (TA Instruments) under a nitrogen atmosphere. FT-IR spectra in attenuated total reflection (ATR) mode were obtained on a Jasco FT/IR-4100 spectrometer. Elemental analysis was performed at Organic Chemistry Research Center, Sogang University (Seoul, Korea) by using EA1112 (CE Instruments, Italy). Powder X-ray diffraction (PXRD) spectra were obtained with a Bruker D8 Focus diffractometer (40 kV, 30 mA, Step size = 0.02°). Optical microscopic images were collected on a Nikon Eclipse LV100POL microscope equipped with a DS-Fi1 CCD camera. The cryogenic volumetric N_2 adsorption-desorption analysis was performed on a Belsorp-miniII at 77 K (BEL Japan). The as-prepared **I** was immersed in chloroform for solvent exchange at least for 3 d. The solvent-exchanged **I** was dried at 393 K under high vacuum for 2 h. Low pressure volumetric CO_2 adsorption measurements were performed on a Belsorp-miniII at 196 K (2-propanol/dry ice bath). Temperature-programmed desorption analysis using CO_2 probe (CO_2-TPD) was performed on a Belcat-B chemisorption analyzer (BEL Japan). The solvent-exchanged **I** was dried at 393 K under high vacuum for 2 h. The activated **I** was treated with a mixture of CO_2/He (10% CO_2) at 303 K for 1 h (flow rate = 60 mL min⁻¹). Then, the sample was purged with He for 1 h (flow rate = 60 mL min⁻¹). The CO_2-TPD profile was obtained with gradual increase of temperature (ramping rate = 10°C min⁻¹).

Preparation of $[EMIM][In(ABDC)_2] \cdot DEF \cdot H_2O$ (I)

$InCl_3$ (0.0111 g, 0.05 mmol), azobenzene-4,4'-dicarboxylic acid (0.0270 g, 0.1 mmol), and 1-ethyl-3-methylimidazolium tetrafluoroborate (0.0099 g, 0.05 mmol) were dissolved in 5 mL of DEF. The reaction mixture was sealed in a screw-capped vial and stored at 120°C for 7 d. After the reaction, the reaction mixture was cooled down to room temperature. The red crystals were retrieved by filtration, washed with DEF, and air-dried (0.015 g,

34%). Anal. Calcd. for $C_{39}H_{40}InN_7O_{10}$ (F. wt. 881.61): C, 53.13; H, 4.57; N, 11.12. Found: C, 53.05; H, 4.77; N, 10.71.

X-Ray Crystallography

The X-ray diffraction data for **I** were collected on a Bruker APEX-II diffractometer equipped with a monochromator in a Mo Kα (λ = 0.71073 Å) incident beam. A crystal of **I** was mounted on a glass fiber and collected data at room temperature. The CCD data were integrated and scaled using the Bruker-SAINT software package, and the structure was solved and refined using SHEXL-2013 (Sheldrick, 2015). All hydrogen atoms were placed in the calculated positions. SQUEEZE/PLATON was used in structural refinement in X-ray experiment. The crystallographic data for **I** are listed in **Table 1**. The selected bond distances are listed in **Table S1**. Structural information was deposited at the Cambridge Crystallographic Data Centre (CCDC reference number is 1904040 for **I**).
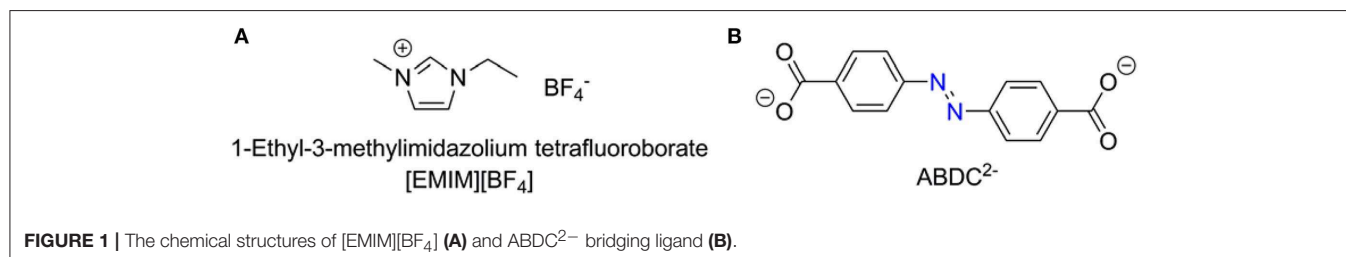
RESULTS AND DISCUSSION

Thermal reaction of the mixture of $InCl_3$, azobenzene-4,4'-dicarboxylic acid (H_2ABDC), and 1-ethyl-3-methylimidazolium tetrafluoroborate ([EMIM][BF$_4$]) dissolved in *N,N*-diethylformamide (DEF) at 120°C afforded the red parallelogram shaped crystals formulated as [EMIM][In(ABDC)$_2$]·DEF·H_2O (**I**) (**Figure S1**). The chemical structures of the room temperature ionic liquid (RTIL), [EMIM][BF$_4$], and the ditopic carboxylate-based $ABDC^{2-}$ bridging ligand are shown in **Figure 1**. Several initial attempts to prepare In-ABDC MOF without the RTIL-based auxiliary counter-cation (EMIM$^+$) in *N,N*-dimethylformamide (DMF) or DEF did not give good quality of crystals as depicted in **Figures 2a,b**. Both $Me_2NH_2^+$ and $Et_2NH_2^+$ directly derived from DMF or DEF solvents may not be suitable for the generation of stable framework structures. $Me_2NH_2^+$ and $Et_2NH_2^+$ ions are thought to be generated by thermal decomposition of DMF or DEF, respectively (Gu et al., 2012). Contrarily, as tetraethylammonium bromide (TEAB) was added into the reaction mixture of DEF, good red block crystals

TABLE 1 | Crystallographic data for **I**.

	I
Empirical formula	$C_{28}H_{16}InN_4O_8$
Formula weight	651.27
Temperature (K)	296(2)
Wavelength (Å)	0.71073
Space group	*C* 2/*c*
a (Å)	43.239 (3)
b (Å)	24.4273 (13)
c (Å)	32.207 (2)
α (°)	90.00
β (°)	131.949 (6)
γ (°)	90.00
Volume (Å^3)	25300 (3)
Z	4
Density (calc.) (Mg/m^3)	0.171
Absorption coeff. (mm^{-1})	0.100
Crystal size (mm)	0.20 × 0.20 × 0.15
Reflections collected	341570
Independent reflections	21976 [*R*(int) = 0.2097]
Data/restraints/parameters	21976/40/174
Goodness-of-fit on F^2	1.029
Final *R* indices [*I* > 2σ(*I*)]	$R_1 = 0.1433$, w$R_2 = 0.3262$
R indices (all data)	$R_1 = 0.1857$, w$R_2 = 0.3565$
Largest diff. peak and hole (e.Å^{-3})	2.387 and −2.128
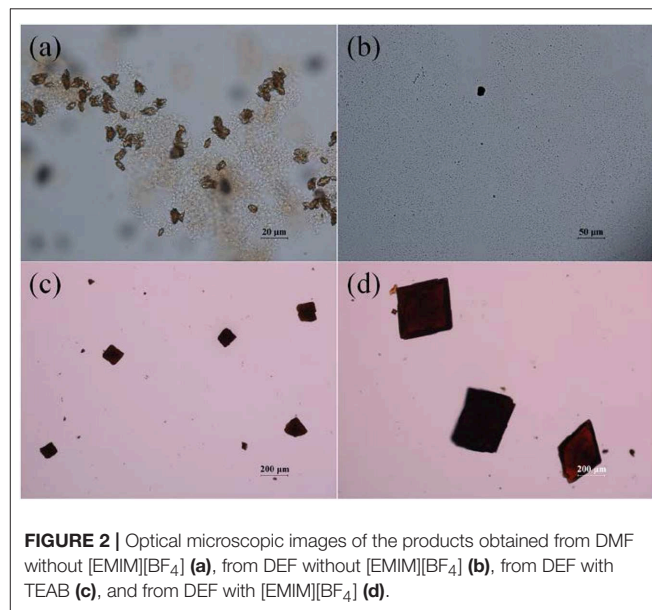
FIGURE 2 | Optical microscopic images of the products obtained from DMF without [EMIM][BF$_4$] **(a)**, from DEF without [EMIM][BF$_4$] **(b)**, from DEF with TEAB **(c)**, and from DEF with [EMIM][BF$_4$] **(d)**.

FIGURE 1 | The chemical structures of [EMIM][BF$_4$] **(A)** and $ABDC^{2-}$ bridging ligand **(B)**.
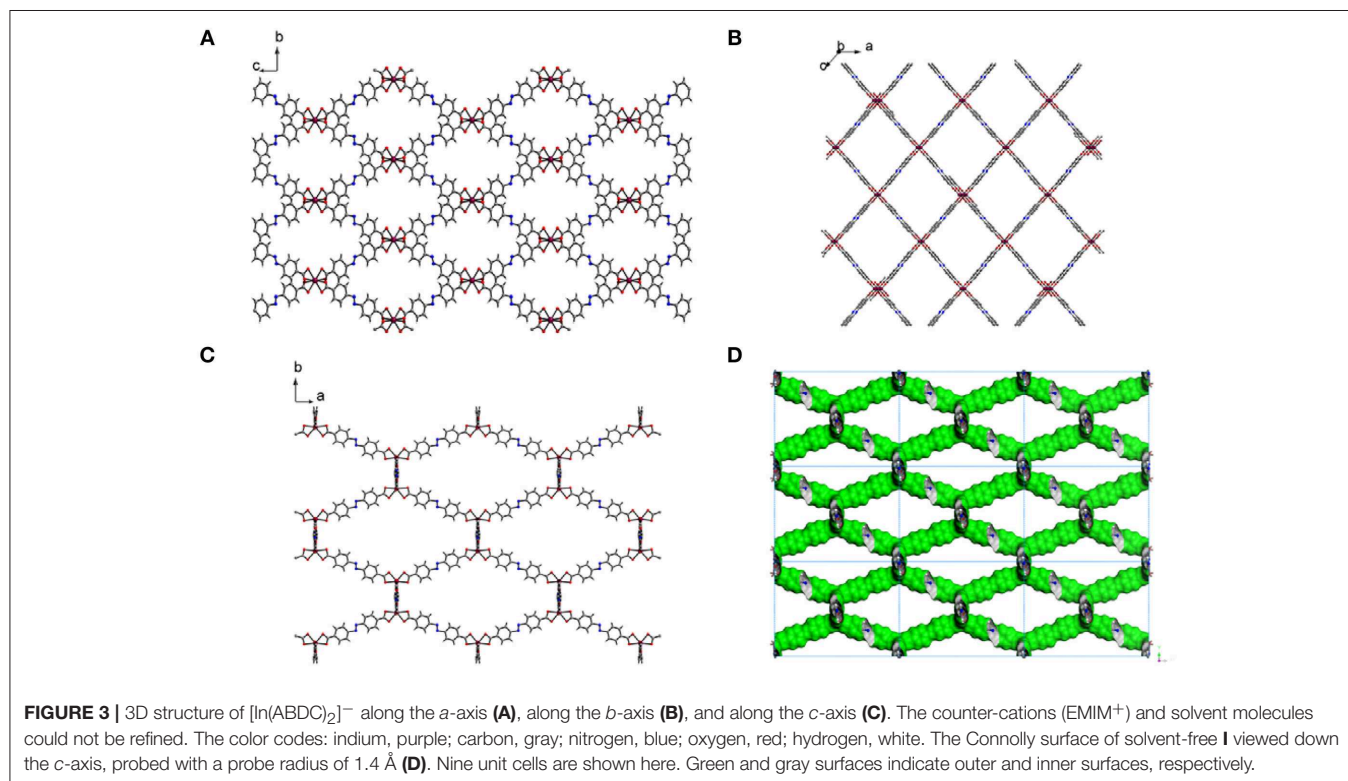
were obtained as shown in **Figure 2c**. Despite its seemingly good quality for X-ray diffraction, the crystal size was too small to get refinable diffraction data. Then, a RTIL-based [EMIM][BF$_4$] was chosen and added into the reaction mixture of DEF solution to lead to parallelogram shaped large X-ray quality crystals of **I** after thermal reaction at 120°C for 7 d (**Figure 2d**). It is noteworthy to mention that the specific type of counter-cation is important for the formation of good quality crystals of **I**.

Fourier-transform infrared (FT-IR) spectrum of the free H$_2$ABDC ligand showed strong C=O and N=N stretching frequencies at 1,681 and 1,424 cm^{-1}, respectively, while crystals of **I** showed C=O and N=N stretching frequencies at 1,662 and 1,414 cm^{-1}, respectively (**Figure S2**). The lowering of C=O stretching frequency clearly indicates the coordination of carboxylate to In^{III} ion. **I** crystallizes in the *C2/c* space group. As depicted in **Figure 3**, ABDC^{2-} ligands bridge In^{III} ions to form a 3D framework. The asymmetric unit contains an In^{III} ion and two ABDC^{2-} ligands (**Figure 4**). **I** contains a EMIM$^+$ cation to compensate the charge of the pseudotetrahedral anionic node, [In(O$_2$CR)$_4$]$^-$, constructed by four carboxylate ligands chelated to an In^{III} ion. The solvent molecules and EMIM$^+$ ions were not refined because they were highly disordered, and the elemental analysis provided the total formula of **I**. An In^{III} ion is 8-coordinated, and geometry of an In^{III} node is pseudotetrahedral constructed by four ABDC^{2-} ligands. The structure indicated a 4-connected uninodal net with Schläfli symbol of 6^6 (**dia**) assuming an In^{III} ion act as a node without any simplification based on ToposPro analysis (ESI) (Blatov et al., 2004). The cation and solvent-free **I** indicated 92.4 % of the void volume based on
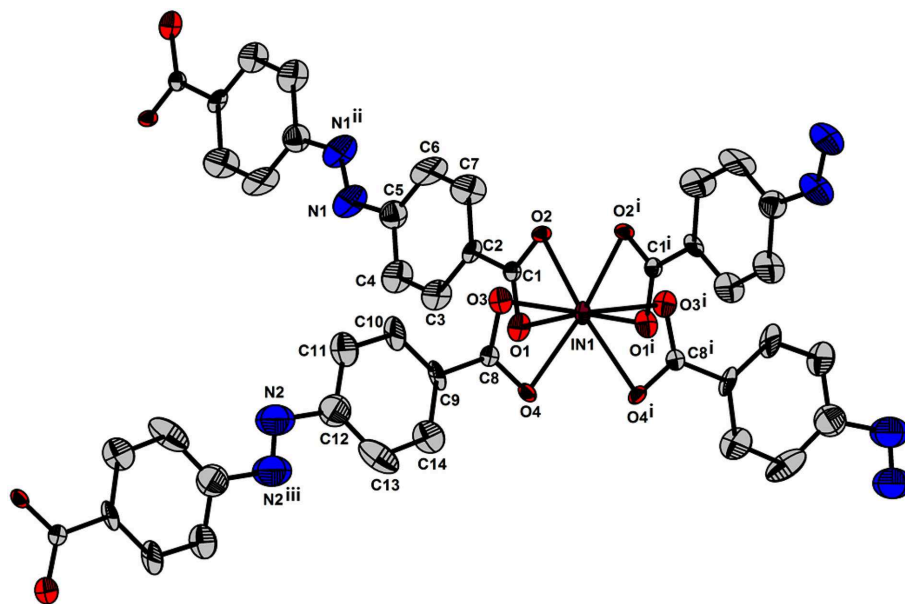
PLATON analysis (Spek, 2004). The real potential void volume should be smaller than the calculated value due to the presence of the counter-cations.

Since the potential solvate molecules in the pores of as-prepared **I** could not be refined by X-ray study, they were characterized by elemental analysis and thermogravimetric analysis (TGA). One DEF and one water molecules were found based on these analyses. The thermal behavior of as-prepared **I** under continuous flow of nitrogen gas indicated that clear loss of these solvate molecules at 250°C as shown in **Figure S3A**. Upon the increase of temperature, gradual weight loss occurred due to the decomposition of EMIM$^+$ counter-cation. After that, rapid decomposition of the framework was observed until around 500°C. The bulk purity of the as-prepared **I** was further investigated by powder X-ray diffraction (PXRD) study as shown in **Figure 5**. The diffraction pattern of the as-prepared **I** agrees well with the simulated one from the X-ray data except the (110) peak. Interestingly, the (110) diffraction plane is almost completely overlapped with (11-1) plane (**Figure S4**). The 2θ angles of (110) and (11-1) are 4.539° and 4.545°, respectively. We speculate that these two diffraction planes with very similar *d*-spacing values result in accidental extinction of the peaks (Lund et al., 2010). In other words, the two diffracted beams happen to destructively interfere each other. So, we could not observe these overlapped peaks despite good elemental analysis, TGA, and X-ray crystal data.

The crystal structure of 3D framework **I** indicated well-defined open channels fully accessible in any directions as depicted in **Figure 3**. Large and small hexagon shaped channels

FIGURE 3 | 3D structure of [In(ABDC)$_2$]$^-$ along the *a*-axis **(A)**, along the *b*-axis **(B)**, and along the *c*-axis **(C)**. The counter-cations (EMIM$^+$) and solvent molecules could not be refined. The color codes: indium, purple; carbon, gray; nitrogen, blue; oxygen, red; hydrogen, white. The Connolly surface of solvent-free **I** viewed down the *c*-axis, probed with a probe radius of 1.4 Å **(D)**. Nine unit cells are shown here. Green and gray surfaces indicate outer and inner surfaces, respectively.

FIGURE 4 | Environment around the anionic pseudotetraheral [In(ABDC)$_2$]$^-$ node of **I**. Displacement ellipsoids are shown at the 30% probability level. All hydrogen atoms were omitted for clarity. Symmetry operations: (i) 1–x, y, 1.5–z, (ii) 1–x, 1–y, 2–z, and (iii) 1.5–x, 0.5–y, 2–z.
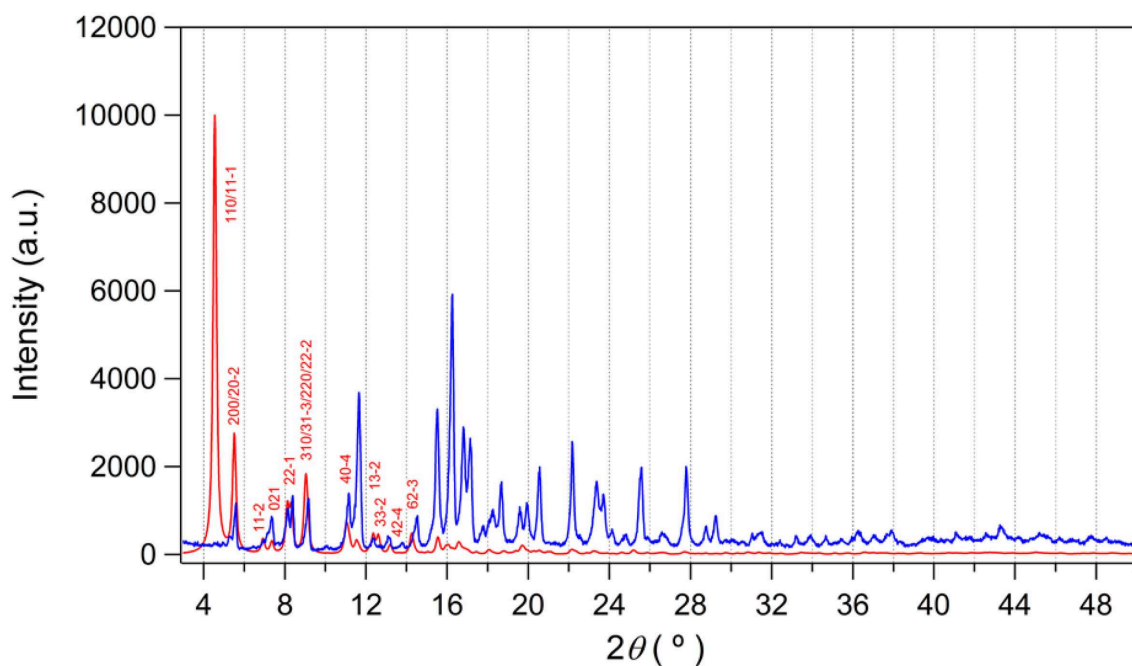
FIGURE 5 | PXRD pattern of as-prepared **I** (blue) and simulated data (red). The simulated pattern is calculated from X-ray structure using Mercury (ver. 4.1.0) with a full-width half maximum (FWHM) value of 0.2. No preferred orientation is considered.

are formed along the *c*-axis and *a*-axis, respectively, and square grid channels are formed along the *b*-axis. The PXRD pattern of the dried sample showed almost identical pattern compared to that of the as-prepared **I** (**Figure S3B**) and this indicated the framework did not collapse during desolvation process. Thus,

the permanent porosity of solvent-free **I** was evaluated by a standard volumetric N$_2$ adsorption/desorption measurement at 77 K. The solvent-exchanged **I** was dried at 120°C under high vacuum before measurement. The N$_2$ adsorption isotherm is a typical Type I isotherm indicative of microporous material

as shown in **Figure 6A**. Despite the seemingly large void space shown **Figure 3**, the presence of a rather bulky $EMIM^+$ counter-cations renders the pore dimension belongs to microporous range (<2 nm). The initial adsorption at low pressure region rapidly increased and then maintained almost constant values before the second rapid increase at high pressure region ($P/P_0 > 0.9$). There is slight hysteresis between adsorption and desorption branches. The Brunauer-Emmett-Teller (BET) surface area is 307 m^2 g^{-1} ($0 < P/P_0 < 0.142$) and the pore volume is 0.38 cm^3 g^{-1}. The Horváth-Kawazoe (HK) micropore dimension is 0.64 nm (**Figure S5**). Additional porosity with relatively small distribution was also observed at 0.99 nm. Thus, **I** can be considered as a bimodal microporous material.

Although the measured BET surface area is relatively low level, the Lewis basic azo groups are fully open toward the channels. Lewis basic sites are known to be beneficial for stronger interaction between framework and CO_2 molecules through acid-base interaction (Gu et al., 2010; Kim and Huh, 2016). Therefore, the CO_2 sorption abilities were also investigated at three different temperatures (**Figure 6B**). The CO_2 sorption measurements at 196, 273, and 298 K showed the uptake of 81.3 (3.63 mmol g^{-1}), 31.1 (1.39 mmol g^{-1}), and 16.4 cm^3 g^{-1} (0.73 mmol g^{-1}), respectively. The uptake at 196 K is somewhat high considering its low BET surface area. For comparison purposes, CO_2 uptake amounts for other known MOFs under similar conditions are summarized in **Table S2**. The isosteric heats (Q_{st}) of CO_2 adsorption were also estimated by using the data at 273 and 298 K. The estimated values by the Clausius-Clapeyron equation and by virial fitting method were very similar each other as shown in **Figure 7A**. The low surface coverage heat of CO_2 adsorption was calculated to be −23.3 kJ mol^{-1} based on the Clausius-Clapeyron equation. The value at zero surface coverage was estimated to be −23.8 kJ mol^{-1} by virial method (**Figure S6**). Both values indicate that the heat of adsorption for CO_2 falls in the usual range of values for common MOFs (Hwang et al., 2012; Sumida et al., 2012). The Lewis basic azo moiety may not strongly enhance CO_2 adsorption at low pressure region. Notably, however the values gradually increase upon the increase of adsorption amount of CO_2. The final values, −31.9 and −30.5 kJ mol^{-1}, are remarkably higher than those of low surface coverage values. This may imply that preadsorbed CO_2 molecules inside channels participate in enhancing additional adsorption of newly incoming CO_2 molecules.

The temperature-programmed desorption analysis using CO_2 probe gas (CO_2-TPD) was also performed to estimate the concentration of accessible Lewis basic sites and qualitatively determine the different types of basic sites. The activated **I** was treated with CO_2 as a form of CO_2/He mixture (10% CO_2) at 30°C for 1 h. The CO_2-TPD curve shown in **Figure S7** indicates that there are several desorption signals below 253°C. This range of values has been attributed to weak basic sites (Wang et al., 2017). Furthermore, the total integrated area indicates the concentration of basic sites is about 0.022 mmol g^{-1}. This amount is much smaller than the CO_2 uptake at 298 K (0.73 mmol g^{-1}). Thus, the azo groups are likely to be very weakly basic.
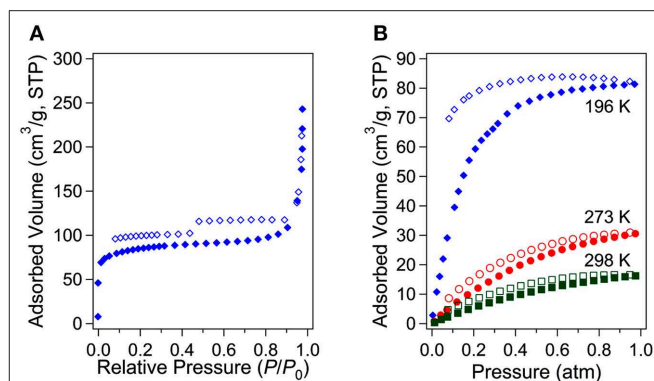
FIGURE 6 | N_2 adsorption/desorption isotherms for the solvent-free **I** at 77 K **(A)** and CO_2 adsorption/desorption isotherms at three different temperatures **(B)**.
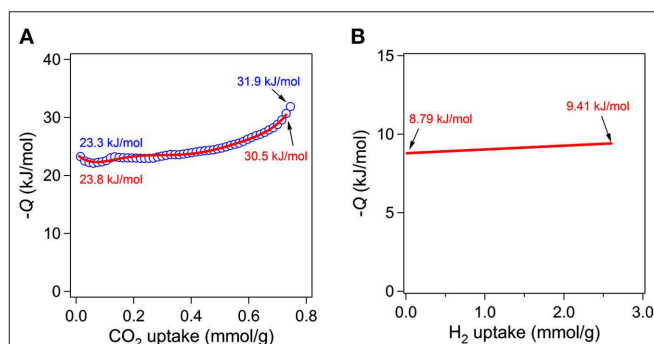
FIGURE 7 | Isosteric heats of CO_2 adsorption as a function of CO_2 uptake estimated from the Clausius-Clapeyron equation (blue open symbols) and virial method (red line) **(A)**. Isosteric heats of H_2 adsorption as a function of H_2 uptake estimated from the virial method **(B)**.

Stimulated from the interesting CO_2 adsorption behaviors and isosteric heats of adsorption for **I**, adsorption of H_2 gas at low pressure was also investigated by volumetric method at 77 and 87 K as depicted in **Figure S8**. The uptake amounts were 102.26 cm^3 g^{-1} (0.92 wt.%) and 58.37 cm^3 g^{-1} (0.53 wt.%) at 77 and 87 K, respectively. Considering the low BET surface area of solvent-free **I**, the uptake of 0.92 wt.% at 77 K is moderately high level. Similar level of values were also observed for $Zn_4O(TMBDC)_3$ (0.89 wt.%, S_{BET} = 1501 m^2 g^{-1}, TMBDC = 2,3,5,6-tetramethylbenzene-1,4-dicarboxylate) (Rowsell et al., 2004), $Mn_3(BDT)_3$ (0.97 wt.%, S_{BET} = 290 $m^2 g^{-1}$, BDT = 1,4-benzeneditetrazolate) (Dincă et al., 2006), and $Na[Ni_3(OH)(SIP)_2]$ (0.94 wt.%, S_{BET} = not available, SIP = 5-sulfoisophthalate) (Dietzel et al., 2006). Interestingly, the BET surface areas of $Zn_4O(TMBDC)_3$ and $Mn_3(BDT)_3$ are quite different each other. Therefore, **I** showed very similar performance with $Mn_3(BDT)_3$. Previously, mesoporous $[Et_2NH_2][In(2,6-NDC)_2]$ (2,6-NDC is 2,6-naphthalenedicarboxylate) with BET surface area of 891.2 m^2 g^{-1} exhibited 1.62 wt.% of H_2 uptake under the same measurement conditions (Huh et al., 2009). Other useful H_2

sorption data for representative MOFs are also summarized in **Table S3**. The isosteric heats of H_2 adsorption were estimated by virial method as given in **Figure 7B** and **Figure S9**. The zero surface coverage value is -8.79 kJ mol^{-1} and this value is relatively high level compared to other known values for common MOFs (Hu and Zhang, 2010). The heats of H_2 adsorption for MOFs are known to be in the range $-3.8 \sim -10.4$ kJ mol^{-1}. The highest values are usually observed for MOFs with openly accessible metal sites which can directly interact with H_2 molecule such as MIL-101(Cr) (Latroche et al., 2006). $Mn_3(BDT)_3$ and $Na[Ni_3(OH)(SIP)_2]$ showed values of -8.4 and -10.4 kJ mol^{-1}, respectively (Dietzel et al., 2006; Dincă et al., 2006). Since **I** does not contain open metal sites, the reason for relatively high isosteric heat of H_2 adsorption is unclear now.

CONCLUSION

The permanently porous 3D In-ABDC MOF, $[EMIM][In(ABDC)_2] \cdot DEF \cdot H_2O$ (**I**), was synthesized successfully and structurally characterized by X-ray diffraction. The RTIL-based counter-cations effectively facilitated the formation of **I**. The 3D framework indicates a 4-connected uninodal net with Schläfli symbol of 6^6 (**dia**). **I** contains a $[EMIM]^+$ cation to compensate the charge of the pseudotetrahedral anionic node, $[In(O_2CR)_4]^-$, constructed by four carboxylate ligands chelated to an In^{III} ion. The N_2 adsorption isotherm is a typical Type I isotherm, and this indicates **I** is a microporous material due to the presence of a rather bulky $[EMIM]^+$ counter-cations despite of large potential void space. The CO_2 sorption ability indicates that preadsorbed CO_2 molecules may participate in enhancing additional adsorption of newly incoming CO_2

molecules. The H_2 adsorption at 77 K also indicated good sorption ability and moderately high isosteric heats of H_2 adsorption. We envision that many new functional In-MOFs can be synthesized by choosing suitable counter-cations for various applications.

DATA AVAILABILITY

The raw data supporting the conclusions of this manuscript will be made available by the authors, without undue reservation, to any qualified researcher.

AUTHOR CONTRIBUTIONS

SH, YK, and S-JK conceived the paper. I-HC, SY, YK, and S-YJ performed the experiments. SH, YK, S-JK, I-HC, and SY interpreted the results. SH and YK wrote the paper.

FUNDING

SUPPLEMENTARY MATERIAL

The Supplementary Material for this article can be found online at: https://www.frontiersin.org/articles/10.3389/fmats.2019.00218/full#supplementary-material

REFERENCES

Aguirre-Díaz, L. M., Reinares-Fisac, D., Iglesias, M., Gutiérrez-Puebla, E., Gándara, F., Snejko, N., et al. (2017). Group 13th metal-organic frameworks and their role in heterogeneous catalysis. *Coord. Chem. Rev.* 335, 1–27. doi: 10.1016/j.ccr.2016.12.003

Baek, J., Rungtaweevoranit, B., Pei, X., Park, M., Fakra, S. C., Liu, Y. S., et al. (2018). Bioinspired metal-organic framework catalysts for selective methane oxidation to methanol. *J. Am. Chem. Soc.* 140, 18208–18216. doi: 10.1021/jacs.8b11525

Beyzavi, M. H., Stephenson, C. J., Liu, Y., Karagiaridi, O., Hupp, J. T., and Farha, O. K. (2015). Metal-organic framework-based catalysts: chemical fixation of CO_2 with epoxides leading to cyclic organic carbonates. *Front. Energy Res.* 3:63. doi: 10.3389/fenrg.2014.00063

Blatov, V. A., Carlucci, L., Ciani, G., and Proserpio, D. M. (2004). Interpenetrating metal-organic and inorganic 3D networks: a computer-aided systematic investigation. Part I. Analysis of the Cambridge structural database. *Cryst. Eng. Comm.* 6, 377–395. doi: 10.1039/b409722j

Chae, H. K., Siberio-Pérez, D. Y., Kim, J., Go, Y., Eddaoudi, M., Matzger, A. J., et al. (2004). A route to high surface area, porosity and inclusion of large molecules in crystals. *Nature* 427, 523–527. doi: 10.1038/nature02311

Chen, S., Zhang, J., Wu, T., Feng, P., and Bu, X. (2009). Multiroute synthesis of porous anionic frameworks and size-tunable extraframework organic cation-controlled gas sorption properties. *J. Am. Chem. Soc.* 131, 16027–16029. doi: 10.1021/ja906302t

Cho, E. Y., Gu, J. M., Choi, I. H., Kim, W. S., Hwang, Y. K., Huh, S., et al. (2014). Encapsulation of various guests by an anionic In-metal-organic framework containing tritopic BTB ligand: crystal structure of Reichardt's dye

captured in an In-metal-organic framework. *Cryst. Growth Des.* 14, 5026–5033. doi: 10.1021/cg5005837

Choi, I.-H., Kim, Y., Lee, D. N., and Huh, S. (2016). Three-dimensional cobalt(II) and cadmium(II) MOFs containing 1,4-naphthalenedicarboxylate: catalytic activity of Cd-MOF. *Polyhedron* 105, 96–103. doi: 10.1016/j.poly.2015.12.022

Chui, S. S. Y., Lo, S. M. F., Charmant, J. P. H., Guy Orpen, A., and Williams, I. D. (1999). A chemically functionalizable nanoporous material $[Cu_3(TMA)_2(H_2O)_3]_n$. *Science* 283, 1148–1150. doi: 10.1126/science.283.5405.1148

Diercks, C. S., Liu, Y., Cordova, K. E., and Yaghi, O. M. (2018). The role of reticular chemistry in the design of CO_2 reduction catalysts. *Nat. Mater.* 17, 301–307. doi: 10.1038/s41563-018-0033-5

Dietzel, P. D. C., Panella, B., Hirscher, M., Blom, R., and Fjellvåg, H. (2006). Hydrogen adsorption in a nickel based coordination polymer with open metal sites in the cylindrical cavities of the desolvated framework. *Chem. Commun.* 959–961. doi: 10.1039/b515434k

Dincă, M., Yu, A. F., and Long, J. R. (2006). Microporous metal-organic frameworks incorporating 1,4-benzeneditetrazolate: Syntheses, structures, and hydrogen storage properties. *J. Am. Chem. Soc.* 128, 8904–8913. doi: 10.1021/ja061716i

Farha, O. K., and Hupp, J. T. (2010). Rational design, synthesis, purification, and activation of metal-organic framework materials. *Acc. Chem. Res.* 43, 1166–1175. doi: 10.1021/ar1000617

Flaig, R. W., Osborn Popp, T. M., Fracaroli, A. M., Kapustin, E. A., Kalmutzki, M. J., Altamimi, R. M., et al. (2017). The chemistry of CO_2 capture in an amine-functionalized metal-organic framework under dry and humid conditions. *J. Am. Chem. Soc.* 139, 12125–12128. doi: 10.1021/jacs.7b06382

Foo, M. L., Matsuda, R., and Kitagawa, S. (2014). Functional hybrid porous coordination polymers. *Chem. Mater.* 26, 310–322. doi: 10.1021/cm402136z

Fracaroli, A. M., Furukawa, H., Suzuki, M., Dodd, M., Okajima, S., Gándara, F., et al. (2014). Metal-organic frameworks with precisely designed interior for carbon dioxide capture in the presence of water. *J. Am. Chem. Soc.* 136, 8863–8866. doi: 10.1021/ja503296c

Furukawa, H., Cordova, K. E., O'Keeffe, M., and Yaghi, O. M. (2013). The chemistry and applications of metal-organic frameworks. *Science* 341:1230444. doi: 10.1126/science.1230444

Gong, L. L., Feng, X. F., and Luo, F. (2015). Novel azo-metal-organic framework showing a 10-connected bct net, breathing behavior, and unique photoswitching behavior toward CO_2. *Inorg. Chem.* 54, 11587–11589. doi: 10.1021/acs.inorgchem.5b02037

Grigoropoulos, A., Whitehead, G. F. S., Perret, N., Katsoulidis, A. P., Chadwick, F. M., Davies, R. P., et al. (2016). Encapsulation of an organometallic cationic catalyst by direct exchange into an anionic MOF. *Chem. Sci.* 7, 2037–2050. doi: 10.1039/c5sc03494a

Gu, J.-M., Kim, S. J., Kim, Y., and Huh, S. (2012). Structural isomerism of an anionic nanoporous In-MOF with interpenetrated diamond-like topology. *Cryst. Eng. Comm.* 14, 1819–1824. doi: 10.1039/c2ce06538j

Gu, J. M., Kim, W. S., and Huh, S. (2011). Size-dependent catalysis by DABCO-functionalized Zn-MOF with one-dimensional channels. *Dalton Trans.* 40, 10826–10829. doi: 10.1039/c1dt11274k

Gu, J. M., Kwon, T. H., Park, J. H., and Huh, S. (2010). DABCO-functionalized metal-organic framework bearing a C_{2h}-symmetric terphenyl dicarboxylate linker. *Dalton Trans.* 39, 5608–5610. doi: 10.1039/c0dt00392a

Hakimifar, A., and Morsali, A. (2019). Urea-based metal-organic frameworks as high and fast adsorbent for Hg^{2+} and Pb^{2+} removal from water. *Inorg. Chem.* 58, 180–187. doi: 10.1021/acs.inorgchem.8b02133

He, H., Perman, J. A., Zhu, G., and Ma, S. (2016). Metal-organic frameworks for CO_2 chemical transformations. *Small* 12, 6309–6324. doi: 10.1002/smll.201602711

Hu, Y. H., and Zhang, L. (2010). Hydrogen storage in metal-organic frameworks. *Adv. Mater.* 22, E117–E130. doi: 10.1002/adma.200902096

Huang, Y., Lin, Z., Fu, H., Wang, F., Shen, M., Wang, X., et al. (2014). Porous anionic indium-organic framework with enhanced gas and vapor adsorption and separation ability. *ChemSusChem* 7, 2647–2653. doi: 10.1002/cssc.201402206

Huh, S. (2019). Direct catalytic conversion of CO_2 to cyclic organic carbonates under mild reaction conditions by metal-organic frameworks. *Catalysts* 9:34. doi: 10.3390/catal9010034

Huh, S., Kwon, T. H., Park, N., Kim, S. J., and Kim, Y. (2009). Nanoporous In-MOF with multiple one-dimensional pores. *Chem. Commun.* 2009, 4953–4955. doi: 10.1039/b905138d

Hwang, I. H., Bae, J. M., Kim, W. S., Jo, Y. D., Kim, C., Kim, Y., et al. (2012). Bifunctional 3D Cu-MOFs containing glutarates and bipyridyl ligands: selective CO_2 sorption and heterogeneous catalysis. *Dalton Trans.* 41, 12759–12765. doi: 10.1039/c2dt31427d

Johnson, J. A., Zhang, X., Zhang, X., and Zhang, J. (2014). Recent advances in ionic metal-organic frameworks: design, synthesis, and application. *Curr. Org. Chem.* 18, 1973–2001. doi: 10.2174/1385272819666140514005108

Karagiaridi, O., Bury, W., Mondloch, J. E., Hupp, J. T., and Farha, O. K. (2014). Solvent-assisted linker exchange: an alternative to the *de novo* synthesis of unattainable metal-organic frameworks. *Angew. Chem. Int. Ed.* 53, 4530–4540. doi: 10.1002/anie.201306923

Kim, H.-C., Huh, S., Kim, S. J., and Kim, Y. (2017). Selective carbon dioxide sorption and heterogeneous catalysis by a new 3D Zn-MOF with nitrogen-rich 1D channels. *Sci. Rep.* 7:17185. doi: 10.1038/s41598-017-17584-8

Kim, H.-C., Huh, S., Lee, D. N., and Kim, Y. (2018). Selective carbon dioxide sorption by a new breathing three-dimensional Zn-MOF with Lewis basic nitrogen-rich channels. *Dalton Trans.* 47, 4820–4826. doi: 10.1039/c7dt04134a

Kim, W.-S., Lee, K. Y., Ryu, E. H., Gu, J. M., Kim, Y., Lee, S. J., et al. (2013). Catalytic transesterifications by a Zn-bisSalen MOF containing open pyridyl groups inside 1D channels. *Eur. J. Inorg. Chem.* 2013, 4228–4233. doi: 10.1002/ejic.201300208

Kim, Y., and Huh, S. (2016). Pore engineering of metal-organic frameworks: introduction of chemically accessible Lewis basic sites inside MOF channels. *CrystEngComm* 18, 3524–3550. doi: 10.1039/c6ce00612d

Latroche, M., Surblé, S., Serre, C., Mellot-Draznieks, C., Llewellyn, P. L., Lee, J. H., et al. (2006). Hydrogen storage in the giant-pore metal-organic frameworks MIL-100 and MIL-101. *Angew. Chem. Int. Ed.* 45, 8227–8231. doi: 10.1002/anie.200600105

Li, G. P., Zhang, K., Zhang, P. F., Liu, W. N., Tong, W. Q., Hou, L., et al. (2019). Thiol-functionalized pores via post-synthesis modification in a metal-organic framework with selective removal of Hg(II) in water. *Inorg. Chem.* 58, 3409–3415. doi: 10.1021/acs.inorgchem.8b03505

Li, H., Eddaoudi, M., O'Keeffe, M., and Yaghi, O. M. (1999). Design and synthesis of an exceptionally stable and highly porous metal-organic framework. *Nature* 402, 276–279. doi: 10.1038/46248

Li, X., Chen, D., Liu, Y., Yu, Z., Xia, Q., Xing, H., et al. (2016). Anthracene-based indium metal-organic framework as a promising photosensitizer for visible-light-induced atom transfer radical polymerization. *CrystEngComm* 18, 3696–3702. doi: 10.1039/c6ce00465b

Lin, Z.-J., Liu, T.-F., Huang, Y. B., Lü, J., and Cao, R. (2012). A guest-dependent approach to retain permanent pores in flexible metal-organic frameworks by cation exchange. *Chem. Eur. J.* 18, 7896–7902. doi: 10.1002/chem.201200137

Lin, Z. Z., Jiang, F. L., Chen, L., Yue, C.-Y., Yuan, D. Q., Lan, A. J., et al. (2007). A highly symmetric porous framework with multi-intersecting open channels. *Cryst. Growth Des.* 7, 1712–1715. doi: 10.1021/cg060732o

Liu, C., Zeng, C., Luo, T.-Y., Merg, A. D., Jin, R., and Rosi, N. L. (2016). Establishing porosity gradients within metal-organic frameworks using partial postsynthetic ligand exchange. *J. Am. Chem. Soc.* 138, 12045–12048. doi: 10.1021/jacs.6b07445

Lund, K., Muroyama, N., and Terasaki, O. (2010). Accidental extinction in powder XRD intensity of porous crystals: Mesoporous carbon crystal CMK-5 and layered zeolite-nanosheets, *Micropor. Mesopor. Mater.* 128, 71–77. doi: 10.1016/j.micromeso.2009.08.004

Lyndon, R., Konstas, K., Ladewig, B. P., Southon, P. D., Kepert, C. J., and Hill, M. R. (2013). Dynamic photo-switching in metal-organic frameworks as a route to low-energy carbon dioxide capture and release. *Angew. Chem. Int. Ed.* 52, 3695–3698. doi: 10.1002/anie.201206359

Maina, J. W., Pozo-Gonzalo, C., Kong, L., Schütz, J., Hill, M., and Dumée, L. F. (2017). Metal organic framework based catalysts for CO_2 conversion. *Mater. Horiz.* 4, 345–361. doi: 10.1039/c6mh00484a

McDonald, T. M., Mason, J. A., Kong, X., Bloch, E. D., Gygi, D., Dani, A., et al. (2015). Cooperative insertion of CO_2 in diamine-appended metal-organic frameworks. *Nature* 519, 303–308. doi: 10.1038/nature14327

Mihaly, J. J., Zeller, M., and Genna, D. T. (2016). Ion-directed synthesis of indium-derived 2,5-thiophenedicarboxylate metal-organic frameworks: tuning framework dimensionality. *Cryst. Growth Des.* 16, 1550–1558. doi: 10.1021/acs.cgd.5b01680

Nguyen, H. G. T., Weston, M. H., Sarjeant, A. A., Gardner, D. M., An, Z., Carmieli, R., et al. (2013). Design, synthesis, characterization, and catalytic properties of a large-pore metal-organic framework possessing single-site vanadyl(monocatecholate) moieties. *Cryst. Growth Des.* 13, 3528–3534. doi: 10.1021/cg400500t

Nguyen, V. H., Nguyen, N. P. T., Nguyen, T. T. N., Le, T. T. T., Le, V. N., Nguyen, Q. C., et al. (2011). Synthesis and characterization of zinc-organic frameworks with 1,4-benzenedicarboxylic acid and azobenzene-4,4'-dicarboxylic acid. *Adv. Nat. Sci. Nanosci. Nanotechnol.* 2:025008. doi: 10.1088/2043-6262/2/2/025008

Phang, W. J., Jo, H., Lee, W. R., Song, J. H., Yoo, K., Kim, B., et al. (2015). Superprotonic conductivity of a UiO-66 framework functionalized with sulfonic acid groups by facile postsynthetic oxidation. *Angew. Chem. Int. Ed.* 54, 5142–5146. doi: 10.1002/anie.201411703

Phang, W. J., Lee, W. R., Yoo, K., Ryu, D. W., Kim, B., and Hong, C. S. (2014). pH-dependent proton conducting behavior in a metal-organic framework material. *Angew. Chem. Int. Ed.* 53, 8383–8387. doi: 10.1002/anie.201404164

Qin, J.-S., Yuan, S., Wang, Q., Alsalme, A., and Zhou, H.-C. (2017). Mixed-linker strategy for the construction of multifunctional metal-organic frameworks. *J. Mater. Chem. A* 5, 4280–4291. doi: 10.1039/c6ta10281f

Rowsell, J. L. C., Millward, A. R., Park, K. S., and Yaghi, O. M. (2004). Hydrogen sorption in functionalized metal-organic frameworks. *J. Am. Chem. Soc.* 126, 5666–5667. doi: 10.1021/ja049408c

Sheldrick, G. M. (2015). Crystal structure refinement with SHELXL. *Acta Cryst. C* 71, 3–8. doi: 10.1107/S2053229614024218

Spek, A. L. (2004). *PLATON-A Multipurpose Crystallographic Tool*. Utrecht: Utrecht University.

Sumida, K., Rogow, D. L., Mason, J. A., McDonald, T. M., Bloch, E. D., Herm, Z. R., et al. (2012). Carbon dioxide capture in metal-organic frameworks. *Chem. Rev*. 112, 724–781. doi: 10.1021/cr2003272

Sun, J., Weng, L., Zhou, Y., Chen, J., Chen, Z., Liu, Z., et al. (2002). QMOF-1 and QMOF-2: three-dimensional metal-organic open frameworks with a quartzlike topology. *Angew. Chem. Int. Ed*. 41, 4471–4473. doi: 10.1002/1521-3773(20021202)41:23<4471::AID-ANIE4471>3.0.CO;2-9

Wang, D., Zhao, T., Cao, Y., Yao, S., Li, G., Huo, Q., et al. (2014). High performance gas adsorption and separation of natural gas in two microporous metal-organic frameworks with ternary building units. *Chem. Commun*. 50, 8648–8650. doi: 10.1039/c4cc03729d

Wang, P., Feng, J., Zhao, Y., Gu, S., and Liu, J. (2017). MOF derived mesoporous K-ZrO_2 with enhanced basic catalytic performance for Knoevenagel condensations. *RSC Adv*. 7, 55920–55926. doi: 10.1039/c7ra12378g

Xu, X., Yang, F., Han, H., Xu, Y., and Wei, W. (2018). Postsynthetic addition of ligand struts in metal-organic frameworks: effect of syn/anti addition on framework structures with distinct topologies. *Inorg. Chem*. 57, 2369–2372. doi: 10.1021/acs.inorgchem.7b02899

Yang, Q., Wang, B., Chen, Y., Xie, Y., and Li, J. (2019). An anionic In(III)-based metal-organic framework with Lewis basic sites for the selective adsorption and separation of organic cationic dyes. *Chin. Chem. Lett*. 30, 234–238. doi: 10.1016/j.cclet.2018.03.023

Yang, X., Yuan, S., Zou, L., Drake, H., Zhang, Y., Qin, J., et al. (2018). One-step synthesis of hybrid core-shell metal-organic frameworks. *Angew. Chem. Int. Ed*. 57, 3927–3932. doi: 10.1002/anie.201710019

Yu, J., Cui, Y., Wu, C., Yang, Y., Wang, Z., O'Keeffe, M., et al. (2012). Second-order nonlinear optical activity induced by ordered dipolar chromophores confined in the pores of an anionic metal-organic framework. *Angew. Chem. Int. Ed*. 51, 10542–10545. doi: 10.1002/anie.201204160

Yuan, S., Zou, L., J.-S., Qin, Li, J., Huang, L., Feng, L., et al. (2017). Construction of hierarchically porous metal-organic frameworks through linker labilization. *Nat. Commun*. 8:15356. doi: 10.1038/ncomms15356

Zhao, N., Sun, F., Zhang, N., and Zhu, G. (2017). Novel pyrene-based anionic metal-organic framework for efficient organic dye elimination. *Cryst. Growth Des*. 17, 2453–2457. doi: 10.1021/acs.cgd.6b01864

Zhao, X., Mao, C., Luong, K. T., Lin, Q., Zhai, Q.-G., Feng, P., et al. (2016). Framework cationization by preemptive coordination of open metal sites for anion-exchange encapsulation of nucleotides and coenzymes. *Angew. Chem. Int. Ed*. 55, 2768–2772. doi: 10.1002/anie.201510812

Zhao, X., Nguyen, E. T., Hong, A. N., Feng, P., and Bu, X. (2018). Chiral isocamphoric acid: founding a large family of homochiral porous materials. *Angew. Chem. Int. Ed*. 57, 7101–7105. doi: 10.1002/anie.201802911

Zheng, B., Bai, J., Duan, J., Wojtas, L., and Zaworotko, M. J. (2011). Enhanced CO_2 binding affinity of a high-uptake rht-type metal-organic framework decorated with acylamide groups. *J. Am. Chem. Soc*. 133, 748–751. doi: 10.1021/ja110042b

Zheng, S.-T., Zhao, X., Lau, S., Fuhr, A., Feng, P., and Bu, X. (2013). Entrapment of metal clusters in metal-organic framework channels by extended hooks anchored at open metal sites. *J. Am. Chem. Soc*. 135, 10270–10273. doi: 10.1021/ja4044642

Zhu, L., Liu, X. Q., Jiang, H. L., and Sun, L. B. (2017). Metal-organic frameworks for heterogeneous basic catalysis. *Chem. Rev*. 117, 8129–8176. doi: 10.1021/acs.chemrev.7b00091

Zhuang, J.-L., Lommel, K., Ceglarek, D., Andrusenko, I., Kolb, U., Maracke, S., et al. (2011). Synthesis of a new copper-azobenzene dicarboxylate framework in the form of hierarchical bulk solids and thin films without and with patterning. *Chem. Mater*. 23, 5366–5374. doi: 10.1021/cm2021092